COMPARISON OF SIMULATED FLOW IN A DISCRETE FRACTURE LABORATORY SAMPLE BASED ON MEASURED AVERAGE AND SPATIALLY VARING HYDRAULIC CONDUCTIVITY

Eunjeong Seok and John E. Gale
Fracflow Consultants Inc., 154 Major's Path, St. John's, NL Canada A1A 5A1

ABSTRACT

Fractured rock masses can be characterized by rapid changes in hydraulic conductivity. In this study, the fully characterized pore space geometry for a 0.055 m^2 section of a fracture plane was used to evaluate approaches to developing input parameters for a finite element flow model; average values, random number generated values, and values that reflect the spatial variability of the fracture pore space. Modeled flowrates based on input parameters that reflect the measured spatial variability matched the measured flowrates but not the model flows produced by other input parameters. Clearly, incorporating spatial variability in numerical model inputs provides a more realistic simulation of experimental data than simply assigning averages or random variability to model inputs. The same pore space and flow measurement data were used to demonstrate the scaling-up effect where, for this data set, sub-samples, each, equal to 0.73% of the total sample area and with a combined area equal to 21.78% of the total sample area gave the density and scale (i.e., scale effect) of hydraulic conductivity measurements that were required to obtained a close match between the measured and computed flowrates. The numerical model simulations show that with increasing size of the subsamples the predicted flowrates rapidly converged on the measured flowrates. The spatial variability approach provided in this work, applies equally to both fractured and porous media.

1 INTRODUCTION

In most geological or natural materials, the hydraulic, geophysical and physical properties of the material or geological system at field scales exhibit strong variability. This partially reflects factors such as facies changes in sedimentary rocks, structural variations, or variations in the scale of fracturing in igneous or metamorphic rocks. At a smaller scale, laboratory samples taken from one location can also exhibit strong variability in the measured parameters. This observation was described by Hubbert [1956] as the representative elementary volume (REV) concept (Figure 1). The REV concept, proposes that higher variability in the selected parameter, exists at the smaller sample size but decreases with increasing sample size as more of the parameter variability is captured and averaged by larger samples. Fractures are pervasive in rock masses and are major contributors to the mechanical, hydro-mechanical and transport properties of fractured rock masses. Predicting flow and transport properties of the fractured rock mass is one of the main objectives during planning, designing and constructing underground structures for waste storage or reservoir/aquifer development.

Laboratory and field permeability data compiled and interpreted (Figures 2 and 3) by Brace [1980 and 1984], Clauser [1992], Gale [1993], and Neuman [1994] for both porous and fractured

media, show that the range of permeability values is greatest for small laboratory samples. Compared to the range of permeability values for the laboratory scale samples, the permeability values measured at the borehole scale show a decrease in the range. In addition a smaller range in the permeability values was observed at the largest scale (regional aquifer systems) for which the permeability values were measured or inferred using assumed boundary conditions. Obviously, part of this scaling pattern or sample size effect is contributed by small-scale heterogeneities that become more significant as the size of the sample decreases. In addition, boundary conditions and the lower measurement limits are much more precisely defined in small-scale laboratory tests and generally much more poorly defined in borehole tests, with the heterogeneities generally being averaged over significant lengths of the borehole test interval. While it is not directly recognized in the REV concept or sample size effect, spatially distributed properties or samples frequently show strong spatial variability or structure. Spatial variability may be a key factor which contributes to the observed or assumed sample size effect.

Witherspoon et al. [1979], Raven and Gale [1985], and Gale [1993] among others addressed the sample size effect using stress-hydraulic conductivity relationship with samples of different sizes ranging from 0.1 m to 0.95 m in diameter. In these experiments, the hydraulic conductivity decreased with increasing normal stress for all the samples regardless of size. However, when the hydraulic conductivities under the maximum stress were compared for different sample sizes, the general trend in sample size-hydraulic conductivity relationship could not be established (Figure 4). This may be attributed to comparing experimental data from different rock types and fracture types along with differences in the flow and boundary conditions for each experiment. Therefore, it is imperative to use samples collected from the same rock masses and to conduct tests using similar flow boundary conditions in order to determine if a size effect exists.

Gale [1984] and Raven and Gale [1985] conducted laboratory tests on different sized samples from the same natural fracture plane in a granite and induced fractures from the same granitic rock. Both data sets showed an apparent size effect. Gale [1984] compared the results from the different size samples by comparing the best fit between the aperture and the normalized flowrate where n is the exponent in the cubic law $k = (\rho \cdot g) / (12 \cdot \mu) \cdot (2b)^n$ [Gale, 1984] (Figure 5). The exponent varied as a function of both stress and sample size. For the smaller samples, the exponent ranged from 1.5 to 6.5. With increasing sample size, the exponent generally converged to a value of 3 for samples that were approximately 200 mm in diameter or greater. Since the comparison was based on the averaging produced by the hydraulic tests, both Gale [1984] and Raven and Gale [1985] were not able to determine if the fracture plane samples exhibited any spatial structure or if there were any significant differences between samples that would account for the variations with sample size. The larger variability in conductivity for the smaller sub-samples suggested that there was a spatial variability since the sub-samples were selected from the same fracture plane randomly without overlapping.

Clearly, to determine if a sample size effect exists for discrete fractures, and to determine if a scaling-up relationship can be defined or if the apparent sample size effect is a reflection of variability or spatial variability in key parameters, one needs to develop detailed descriptions or establish databases for the key parameters in the flow system. These databases must include both the flow and transport properties of the fracture plane, or fractured rock mass, or the key parameters that allow one to calculate flow and transport in discrete fractures, such as the

fracture pore space geometry. In addition, one must make those measurements that provide the data needed to identify the role of variability and spatial variability of hydraulic conductivity, at all scales, in controlling flow and transport within a fractured rock mass.

Most rock masses or experimental sites are characterized using a series of point measurements where once a statistically significant sample or description has been obtained it is then extrapolated or extended to describe the entire sample or area of interest. Evaluation of the basic concepts of scale effects and spatial variability and their impact on flow and transport through fractures, requires a fully characterized system. With the available technology, fully characterizing a discrete fractured rock mass is not tenable and if it was feasible, the effort would be very expensive. However, it is feasible to essentially fully characterize a discrete fracture plane at the laboratory or field scale and to use such data sets to evaluate how different approaches to scaling-up, averaging and or assigning spatial variability determine the match between measured flowrates and computed flowrates as well as transport within the discrete fracture planes. In this paper, we present the results of an experimental study [Seok, 2001] on a fracture plane sample, measuring 190 mm by 290 mm, in which the fracture pore space geometry was fully characterized for known normal and shear loads, measured fracture closure and measured flowrates. The experimental data from this experiment were used to conduct a series of numerical experiments to evaluate the use of different procedures for averaging and representing pore space geometry or hydraulic conductivity when developing input parameters for numerical models. These models were then used to compare measured flowrates and computed flowrates for the discrete fracture plane In addition, a limited number of numerical experiments were conducted to evaluate the role of sample size and data density when simulating flow through discrete fracture planes using detailed fracture pore space geometry for comparison with actual flow measurements.

2 MEASURED AND SIMULATED FRACTURE PORE SPACE GEOMETRY AND COMPUTED FRACTURE HYDRAULIC CONDUCTIVITY

2.1 Experimental Design and Pore Space Data

As presented in Seok [2001], a 190 mm diameter granitic core sample containing a section of a fracture plane, oriented parallel to the core axis, was recovered from the Svenk Kärnbränslehantering AB (SKB) Underground Hard Rock Laboratory (HRL) at Äspö, Sweden. Laboratory tests were conducted on this fracture plane sample to determine the coupled hydraulic-mechanical behavior of the fracture plane and to determine the impact of degassing on fracture transmissivity at selected stress levels [Gale, 1999]. This sample was subjected to a number of normal loading and unloading cycles followed by a shear loading cycle. Flow and tracer tests were conducted at selected stress levels on the fracture plane. After the final flow and tracer tests were completed at approximately 10 MPa of normal stress, a room temperature curing resin was injected into the fracture plane. Since the resin was injected under the same stress conditions as those which existed for the final flow and tracer tests, mapping the resin filled pore space allows one to determine the impact of pore space geometry on the flow and transport properties of this discrete fracture. In addition, the fully characterized pore space geometry allows one to evaluate the flow laws that are applicable to flow and transport through a discrete fracture whose walls are in intimate contact under the applied stress condition.

After the resin had fully cured, the sample was unloaded and a section of the rock sample containing the resin bonded fracture plane was obtained by making cuts with a diamond saw parallel to and on both sides of the fracture plane. The final dimensions of the slab for the ÄSPÖ2 sample, that contained the resin impregnated fracture plane, were 290 mm in length, 190 mm in width, and 51 mm in thickness. The pore space mapping procedure consisted of cutting sections perpendicular to the fracture plane, photographing the resin filled fracture plane using a camera mounted on a microscope, and then digitizing the outline of the resin filled fracture plane. Analysis of the fracture pore space data in an earlier study [Fracflow Consultants Inc., 1997] from 10 mm spaced sections showed that the correlation lengths were generally shorter than the 10 mm spacing between the sections that were cut in the previous work. Therefore, additional sections were cut perpendicular to the fracture plane in both the X and Y directions, such that the final section or fracture profile spacing was 5 mm. Photographs of the resin filled pore space and contact areas within each section were joined together to form a continuous profile of each section. The traces of the fracture pore space and the asperity contacts, or lengths, along each section were digitized to provide data on the spatial distribution of the pore space geometry. The separation distance or aperture between the top wall and the bottom wall of each fracture section was computed at 0.4 mm intervals along each trace by subtracting the bottom profile from the top profile. Asperity contact lengths were mapped separately and recorded as line segments with zero aperture. Similarly, areas of each fracture plane that were filled with rock and fracture mineral debris impregnated by resin were identified and mapped separately. This fracture or pore space mapping procedure generated a total of 20,152 data points, apertures, contact lengths, and resin impregnated crushed material for the ÄSPÖ2 fracture plane sample. The detailed experimental and aperture mapping procedures and specifications can be found in Seok [2001].

The pore space data for the ÄSPÖ2 sample, which included the contact points and the open pore spaces, enabled one to develop a statistical description of the pore space geometry. These statistics were then used to describe the spatial structure of the fracture pore space. The histogram of the measured pore space data, with 0.04 mm class intervals, is presented in Figure 6(a). This histogram can be considered bimodal based on the two peaks present in the distribution when one includes contact area as well as the open pore space data; one peak centered on the 0 to 0.04 aperture range (contact area) and the other centered on the 0.12 to 0.16 mm aperture range (open pore space data). Key parameters and statistics for the open pore space and contact area distributions are provided in Table 1. The pore spaces smaller than or equal to 0.001 mm, based on point measurements, were treated as contact sections/lengths and are included in the 0 to 0.04 mm class interval. The normal stress on the fracture plane which was maintained at 10 MPa while the resin was being injected produced a contact area of 24.95%, based on the measured contact lengths. The histograms of the natural logarithm of the open pore space data for the ÄSPÖ2 sample are characterized by lognormal distribution (Figure 6(b)) with a negative skewness (Table 1) as shown by the long tail for the smaller pore spaces. An exponential model was fitted to the semi-variogram by varying the sill and range in the exponential model to minimize the sum of the differences between the measured and model semi-variogram values at the selected lag distances.

A geostatistical model was used with these measured pore space data to generate a regular grid of pore space data for the entire model region (fracture plane) that were used as numerical model

input data for simulating flow and transport through the pore space of the fracture plane sample. The basic statistics and semi-variogram properties were compared to ensure that each estimation or simulation result reproduced the bimodal nature of the pore space histogram as well as the spatial structure of the fracture plane pore space geometry that existed when the flow tests were conducted.

2.2 Simulation of Pore Space Geometry

To reproduce the spatial structure of the pore space geometry as it existed when the flow and transport tests were conducted, the spatial continuity for the pore space in the sample was evaluated by comparing the semivariogram for the generated pore space with the semivariogram computed using the measured pore space data. Then a pore space geometry with 1 mm by 1 mm regular grid was generated using 'Simulated Annealing' The simulated annealing process accepts a spatial structure in the pore space by perturbing one pair of grid cells in the initial image for each perturbation until the specified characteristics in the objective function are met. Since the basic statistics and the bimodal nature of the histogram of the ÄSPÖ2 sample data set had already been reproduced in the initial image, the objective function consisted of only the semivariogram reproduction. Several combinations of annealing schedules and parameters were applied to the initial images to produce several realizations. Then the semivariogram for each realization was compared to that of the measured data. At the end of this process, one realization was selected based on the degree of fit of the semivariogram to the data set. Figure 7 shows the pore space maps that were generated by the simulated annealing process and the semivariograms that were calculated for the simulated data. The semivariograms of the measured pore space data for the ÄSPÖ2 sample are also plotted in Figure 7(b) for comparison with the semivariograms for the simulated data. Both the semivariogram sill and the range for the annealed pore space map are the same as those of the measured pore space data. However, the semivariograms for the annealed data, for lag distances less than 4 mm, show less variance than those for the measured pore space data. This implies that, for the simulated or annealed pore space data, most data point pairs that have lag distances less than 5 mm have more continuity than the measured pore space data.

2.3 Computing Fracture Hydraulic Conductivity

Flow through fractures is assumed to be controlled by the friction factor versus Reynolds Number relationship (Figure 8) with the basic reference being the parallel plate or cubic law for flow between two, open, smooth parallel plates. However, as noted by a number of other researchers and demonstrated by the percentage of contact area for the ÄSPÖ2 sample, most in-situ fracture walls are in intimate contact, pressed together by the applied effective normal stress and as such natural fractures in a rock mass do not satisfy the assumptions that are inherent in the derivation of the parallel plate flow and transport law. Based on the published literature (Gale, 1999), there appears to be only a few experiments where the friction factor versus Reynolds Number relationship has been evaluated or measured (Figure 8) and these were cases where the rough fracture surfaces were merely touching and hence not in intimate contact. For laminar flow, at low Reynolds Numbers, attempts have been made to correct for the impact of roughness of the fracture walls and the intimate contact between the fracture walls, on the basic flow laws by

introducing a relative roughness term. This approach is adopted in this work to allow the flow through the simulated fracture plane pore space to be compared to the measured flows using an equivalent porous media flow and transport model. The obtained or simulated pore space data from the simulated annealing process were converted to fracture hydraulic conductivities using the equation for the modified parallel plate model,

$$K_f = \frac{\rho \cdot g \cdot (2b)^2}{12 \cdot \mu \cdot \left[1 + 8.8(k/dh)^{1.5}\right]}$$ [Louis, 1969]

where ρ is the fluid density, g is the gravitational acceleration, μ is the dynamic viscosity, $2b$ is the fracture aperture, and k/dh is the relative roughness. For fracture walls that are in intimate contact, the relative roughness (k/dh) is deemed to be 0.5 [Louis, 1969, see Section 1.3.1].

The fracture hydraulic conductivities have to be converted to equivalent porous medium conductivities in order to be used as input parameters in a 3D numerical model that is based on porous media. For the flow model, the volumetric water flow should be the same in the fracture and the model,

$$Q_f = Q_m$$

where, Q_f and Q_m are the volumetric flows in the fracture plane and in the model, respectively. The equation can be rewritten as,

$$K_f \cdot I \cdot A_f = K_m \cdot I \cdot A_m$$

where, K_f and K_m are the conductivities of the fracture plane and the model, respectively, I is the gradient and A_f and A_m are the cross-sectional area of the fracture plane and the model, respectively. The fracture conductivity, K_f, is calculated based on the measured apertures, $2b$, from the resin impregnated samples (Seok, 2001). Since the gradient must be the same between the flow test and the model, the equation reduces to,

$$K_f \cdot 2b \cdot W = K_m \cdot s \cdot W$$

where, s is the spacing in the model and W is the width of the fracture and the model. Therefore, the equivalent porous media model conductivity, K_m, can be calculated using the fracture conductivity as,

$$K_m = K_f \cdot \left(2b / s\right)$$

Finally, the fluid velocity in the flow simulation, when transport simulations are being considered, is approximated to that in the fracture by assigning an appropriate porosity value for the equivalent porous media that is computed from the fracture aperture using an assumed fracture spacing, in this case a 1.0 m fracture spacing.

3 IMPACT OF FRACTURE PERMEABILY CHARACTERIZATION ON COMPUTED FLUX

Hydrogeological models are constructed to allow one to analyze laboratory experiments or evaluate field sites for assessment of environmental, water resources, and water management impacts and issues. Because of the size of most sites of interest and even laboratory experiments, models have to be constructed using sparse data sets due to overall costs, site access and the time frames within which operational and project decisions have to be made.

In laboratory studies, the hydraulic conductivity values are normally computed from the measured flux and one or more measures of the hydraulic gradient across the entire sample or sections of the sample. Similarly, with tracer tests on laboratory samples, the focus is primarily on the boundary conditions with very few, if any, measurements within the flow field.

The input parameters, including hydraulic conductivity, porosity, and hydraulic head, for 3D hydrogeological models of large field sites, are derived from a limited number of borehole measurements, a limited number of aquifer tests, and in some cases drift inflow data. The challenge is to assign the hydraulic properties to the elements or cells in the model such that the model reflects a reasonable representation of the real hydrogeological system.

In constructing 3D hydrogeological models, with multiple layers and different geological units, it is common for modellers to use one value of hydraulic conductivityand porosity to populate the elements or cells in a geological group or a corresponding layer in the model. For instance, the geometric mean of the hydraulic conductivity measurements that were derived from borehole tests is generally used as the hydraulic conductivities in the model. Applying one representative value for a single layer or geological unit over the entire model area, however, generally presents problems for model calibration and will produce results with a high degree of uncertainty, especially in fractured rock systems where the measured properties can vary with location and borehole direction. In this case, the local variation in hydraulic properties and its impact on flux and transport cannot be captured with the averaged hydraulic property value. Geostatistics represent an approach that can be introduced in an attempt to characterize the spatial variability in key hydraulic parameters for the domain or domains of interest. Constructing 3D numerical models in which this spatial variability is reflected in the model input parameters should provide more robust calibration of the model against measured data and reduction in the uncertainty associated with the model predictions. However, the first requirement to test the improvement in groundwater flow model predictions where spatial variability is reflected in the model input parameters is access to a fully or well characterized database for a well-defined flow system or flow field under field or laboratory conditions.

The pore space data that were generated for the ÄSPÖ2 laboratory sample are considered to represent a complete characterization, from a practical perspective, of the apertures that controlled the flow and transport through this section of the fracture plane. This fully characterized section or sample of a fracture plane provided the opportunity to determine the impact of fracture pore space geometry and the resultant hydraulic conductivity characterization on the fracture flux that is computed using a numerical model. Three hydraulic conductivity input data sets were created from the measured aperture and contact/asperity data and used to assign the hydraulic conductivity values to the one millimetre grid cells in the flow model. The three hydraulic conductivity data sets were constructed using: 1) the average or uniform fracture aperture; 2) apertures that were generated from the basic pore space statistics using a random number generator; and 3) apertures that were generated using geostatistics that were computed from the pore space data such that the final aperture or hydraulic conductivity data reflected the underlying spatial variability that had been computed for the fracture plane sample. Since the hydraulic conductivity varies rapidly from cell to cell, the Feflow code [Diersch, 2005] was

tested using simple geometrical models of a fracture plane to confirm that the code correctly simulated the hydraulic head changes that were associated with abrupt change in apertures.

– Data Set 1: Uniform fracture aperture or uniform hydraulic conductivity

The ÄSPÖ2 fracture plane is characterized by highly variable apertures. Duncan et al. [1972] demonstrated how non-uniform apertures could be converted into equivalent uniform apertures for the one-dimensional case using the measured fracture lengths and apertures to compute an equivalent uniform fracture hydraulic conductivity. No direct procedure, however, exists with which to compute equivalent uniform fracture apertures from fracture pore space data for the two-dimensional case and to convert the computed uniform aperture to an equivalent uniform fracture hydraulic conductivity.

To calculate a uniform equivalent porous media hydraulic conductivity for the uniform aperture case, even in the one-dimensional case, one must first calculate the average aperture. The average aperture (arithmetic mean) can be calculated by finding the average width of the open pore space excluding the contact points. For fractures with a significant percentage of contact area, however, this approach would bias the aperture in terms of the larger pores. To ensure that the computed uniform aperture reflected the contact areas, the average value used in this section was calculated using all the available data points including both open pore space and contact points in order to obtain a representative value. The equivalent uniform porous media hydraulic conductivity was computed from this average aperture following the procedures outlined in the previous section. A second uniform aperture (geometric mean) was calculated by taking the average of the natural logarithm of the same set of apertures that were used to compute the average aperture. In both cases, a minimum aperture of 0.001 mm was assigned to the contact areas so that they could be included in the averaging process.

The average hydraulic conductivity value, that was computed from the average apertures, was assigned to each cell or element in the flow model first using the arithmetic mean aperture and then using the mean of the logarithm of the apertures. Table 2 shows the arithmetic and logarithmic average values of the measured data points and corresponding equivalent porous media hydraulic conductivities. Two models were run using each hydraulic conductivity value as the uniform input parameter that was assigned to the entire fracture plane.

– Data Set 2: Randomly distributed hydraulic conductivity

The second approach to populating the cells of numerical models when there is limited field data and or large spatial gaps in the measured data is to use a random number generator, based on the statistics of the original field data distribution, to assign the required hydraulic properties to individual cells or elements. With this approach, the statistics of the input parameters are derived from and match those of the measured data.

In this second approach, the data set that was generated by applying the simulated annealing procedure [Seok, 2001], was used as the model input parameters. This data set had the same basic statistics as the measured pore space data set and the bimodal nature of the measured data set was also maintained (Figure 9). However, this data set that was generated using a random

number generator did not show any significant spatial distribution (Figure 10(a)). The calculated semivariograms and correlograms shown in Figure 10(b) confirm the lack of spatial distribution in this data set.

– Data Set 3: Spatially distributed hydraulic conductivity

The hydraulic conductivity values for fractured rock masses are known to be spatially correlated with the variation in the degree or intensity of fracturing or the underlying structure. For example, in simple layered sedimentary rock structures such as anticlines or synclines, the fracturing is more intense along the crest of anticlines and the trough of synclines than the fracturing along the flanks of both structures. Also, the fracturing appears to be correlated with the overall curvature of the bedrock layers [Gale et al., 1991]. In constructing and executing a 3D model of such structures, assignment of model properties based on either the arithmetic mean, the geometric mean or the harmonic mean of the measured properties, or assignment of the model properties based on a random number generator using the statistics of the field data, will produce significant calibration errors.

The fracture pore space data for the ÄSPÖ2 sample exhibit spatial variability. The simulated annealing application was applied to this last data set. As described in the previous section, this data set was generated using the modified simulated annealing method, so that the spatial correlation of the measured data set was reproduced in the simulated data set while the basic statistics and the histogram of the measured data set were also maintained. One of the pore space maps is shown in Figure 7(a) for comparison with the randomly distributed pore space map that is shown in Figure 10(a).

Table 2 tabulates the numerical model results for this single fracture case for each of the three different methods used to assign the hydraulic properties. When the measured apertures and contact areas were averaged and the equivalent uniform hydraulic conductivity was computed for this average aperture and then assigned to all elements in the model, the computed flux was 1.4 ml/s which is much higher than the measured flux (0.5 ml/s). More important, when the individual apertures and contact areas were first converted to equivalent uniform hydraulic conductivities and the arithmetic average of these hydraulic conductivities was calculated and assigned to each element, the computed flux through the fracture plane was 8.4 ml/s. This reflects the weighting that is provided by the cubic relationship or non-linear relationship that is assumed to exist between fracture aperture and fracture flow, i.e., the large apertures have a much larger impact on the computed flux.

Overall, the only set of hydraulic conductivity data that clearly brackets the measured flux value, is the case where the spatial variability or spatial structure of the hydraulic conductivity distribution has been captured. Obviously, important aspects of the hydraulic conductivity structure of discrete fracture planes that in turn controls the flux and most likely also the transport properties, is lost if one uses an averaging process.

4 HYDRACULIC CONDUCTIVITY SCALE EFFECT

Any review of laboratory- and field-measured flow and transport properties in fractured rocks confirms that these fractured rocks are characterized by a wide range in hydraulic conductivities and fluid/contaminant velocities along with a high degree of anisotropy. This wide range in hydraulic properties presents serious challenges when one is attempting to predict flux and contaminant transport in both saturated and partially saturated fractured rocks systems.

Permeability data (Figure 3) compiled and interpreted by Clauser [1992], for both porous and fractured media, show that the range of hydraulic properties appears to be about 7 to 8 log scales (Log_{10} ranged from -15 to -23 with k in m^2) for small laboratory samples, with the range of the permeability values decreasing as the scale of measurement or sample size increases. However, this reduction in range may be related more to a smaller number of samples for sample sizes greater than 10 cm than to an actual narrowing of the range of permeability values.

Measurements at the borehole scale (Figure 3) usually include test sections of the rock mass that are orders of magnitude larger than most laboratory samples. The borehole measurements show a much wider range in measured values than is shown by the laboratory data. In addition, the average or mid-range values reported by Clauser [1992] are higher than those presented for the laboratory scale samples. Obviously, borehole test sections capture open fractures and discontinuities that are not captured or not well represented in laboratory samples. The regional scale data tabulated by Clauser [1992] are limited in number and each site or area, in most cases, is represented by only one data point. Where more than one data point is available for a given sample or test size, the range is relatively narrow when compared to either the laboratory or borehole scale data, but this may not be significant.

Overall, there appears to be a trend of increasing hydraulic conductivity with increasing sample size up to the 100 m scale, followed by a poorly defined pattern of decreasing hydraulic conductivity at the regional scale where the interpretation of the hydraulic conductivitiesfor these large regional aquifer systems is based on measured and assumed boundary conditions. Changes with sample size or the size of the area being investigated are normally referred to as the “scale effect” and considerable effort has been devoted to developing scaling-up procedures without fully examining the hydraulic conductivity database from which these scale effects are inferred. Gale [1993] added additional laboratory data to the data that were presented by Clauser [1992], for a range of porous and fractured samples, and showed that the range for the mid-range values of permeability for laboratory scale samples could be extended to cover approximately 13 log cycles. Using the mid-range values only, Gale [1993] showed (Figure 2) that the borehole and regional scale values fell within the mid-range of the permeability values that were determined from laboratory data.

Obviously, part of this change with sample size is contributed by small-scale heterogeneities that become more significant as the size of the sample decreases. In addition, test boundary conditions and the lower measurement limits are much more precisely defined in small-scale laboratory samples and generally much more poorly defined or assumed in borehole tests, with the heterogeneities generally being averaged over significant lengths of the borehole test interval.

A comprehensive discussion of how transport properties in porous are assumed to scale is provided by Neuman [1990]. In transport studies, the main focus is usually placed on the

dispersivity of the media or how the contaminant spreads with increase in distance traveled and in the time required to travel over the specified distance rather than on the average fluid or contaminant velocity. In fractured rocks, which are characterized by strong anisotropy and rapid changes in fluid velocity from fracture to fracture, very little data exist with which to assess scale effects from a transport perspective.

In low-permeability fractured rocks, it has been assumed by some investigators that flow and transport are controlled by a number of high-permeability pathways, consisting of or within discrete fractures that are not captured by small-scale laboratory samples [Margolin et al., 1998]. However, large-scale field tests, such as the Stripa macro-permeability experiment (Witherspoon, 2000), did not show any evidence in the measured gradients that would support an interpretation that a few high permeability pathways were dominating the flux into the mine drift. Furthermore, single fracture borehole packer tests in the same rock mass [Gale et al., 1987], while indicating a truncated distribution due to the limits on the measurement of low flowrates, did not show a bimodal fracture transmissivity distribution (Figure 11).

Given the need to determine how to scale-up from laboratory and borehole data sets to simulate and predict flow and transport in volumes of fractured rock that are of interest to a number of investigators, extensive numerical investigations have been conducted [Margolin et al., 1998, among others] to determine how key parameters scale with an increase in the area of interest. Without adequate deterministic fracture-property databases, however, including measured flow and transport properties, with which to calibrate or exercise the available models, it is difficult to validate the various conceptual models of flow in fracture systems along with the appropriate scaling relationships. Databases need to be developed at different scales, and the fracture-pore-space database that is presented here has been used to evaluate scaling relationships at the scale of a single fracture plane.

5 ASSESSING SCALING RELATIONSHIPS USING PORE SPACE DATA - SMALL SCALE FRACTURE

Since the pore space geometry that controls the flow and transport in this fracture plane sample is essentially fully characterized, the concept of scale-effect or scaling-up can be evaluated by selecting a number of small, but different sized, sections from the fracture plane and determining how these sections contribute to flow through the entire fracture plane. This approach allows one to determine how the prediction of the measured fracture flowrate is affected by the size of the sub-sample that is used to populate the hydraulic conductivity distribution for the overall fracture plane.

5.1 Sub-sampling of the Fracture Plane

The fracture plane pore-space geometry was divided into 55,100, 1 mm by 1 mm, grid cells. The overall discrete fracture plane was divided into a series of blocks whose size were the selected sample scale. Each block was numbered sequentially. Thirty block numbers were selected from the entire list of blocks using a random number generation for each sample size. This procedure was repeated for each sub-sample. To demonstrate the role of scale, five different sub-sample

sizes were used (Figure 12): 10 mm by 10 mm (100 mm^2 or 100 grid cells), 15 mm by 15 mm (225 mm^2), 20 mm by 20 mm (400 mm^2), 30 mm by 30 mm (900 mm^2) and 40 mm by 40 mm (1600 mm^2). Figures 13 to 17 show the randomly selected locations for each group of sub-samples. Each group of sub-samples consisted of 30 sub-samples except for the 40 mm by 40 mm samples where only 27 sub-samples were generated due to the limitations imposed by the size of the original fracture plane.

5.2 Flow Simulation

A 3D model using Feflow [Diersch, 2005a] was set up for each sub-sample with a corresponding 1 mm by 1 mm grid size and one layer. Flow in both the X direction (Q_x) and the Y direction (Q_y) were simulated for each sub-sample. As discussed above, the measured pore space or aperture data from the simulated annealing process were converted to fracture hydraulic conductivities using the equation for the modified parallel plate model [Seok, 2001], with a relative roughness of 0.5. The fracture hydraulic conductivities were converted to equivalent porous medium conductivity and assigned as input parameters in the 3D FEFLOW flow and transport model (Diersch, 2005a).

Figure 18 shows a schematic of the flow boundary conditions used in these simulations. The injection head was increased proportional to the sample size so that the hydraulic gradient for each sub-sample was the same. No-flow boundaries were assigned to two sides of the sample and constant head values were assigned to the other two sides. The hydraulic conductivity for each cell was calculated and assigned based on the corresponding aperture. Table 3 shows the basic model geometry and input parameters for each group of sub-samples.

The computed flux was normalized to the hydraulic head. Then, the difference in the model size was compensated by dividing the flux by a ratio of the width to 10 mm. The logarithm of the normalized flux in both the X and Y directions, the mean, standard deviation and variance of the apertures in each sub-sample were computed to enable these five measures to be presented on the same plot (Figure 19) with a vertical axis that ranges from -20 to +10 in log units. The horizontal axis shows the individual sample number within each sample size group. In these individual plots, the aperture data along with the computed flux values were sorted and plotted in terms of increasing mean aperture (i.e., decreasing negative values since all of the mean apertures are less than 1 mm). Figure 19 shows that the degree of variability in the computed flux values decreases with both increase in sample size and with increase in the mean aperture for each sub-sample. Clearly, with sub-sample sizes less than 20 mm by 20 mm, there was a much smaller possibility that the sub-sample would produce a flux value for this section of the fracture plane that was comparable to the measured flux value for the entire sample. The details of the computed flux for each group are also shown in Table 4.

Figure 20 shows the box plots of the computed normalized flux for Q_x and Q_y and the range of mean apertures for each group of sub-samples. The measured flux value is shown as a solid line for reference. The average and median values for the normalized flux (Q*) and apertures for each group are also plotted and the outliers are indicated for each sub-sample group.

The mean computed flux values for both the X and Y directions for the 10 mm and 15 mm sub-samples are lower than the measured flux. The range of flux, defined by the 25 and 75 percentiles, is wide in the smallest sample size and decreases dramatically with increasing sample size.

6 SUMMARY

For the entire fracture plane sample: 1) the simulated flux based on average hydraulic conductivity values and that based on the randomly assigned values did not match the measured value; and 2) the computed flux matched well to the measured flux when the hydraulic conductivities were constrained by the underlying spatial variability over the fracture plane. Characterizing the spatial structure of the underlying hydraulic conductivity data is required if one is to successfully predict flowrates in a given system. Flowrates, predicted using average and/or randomly assigned permeability values to populate an entire model area should not be expected to match the measured flowrates.

Comparison of the computed and measured flux as the sub-sample size was increased showed: 1) smaller sub-samples had greater variability in computed flux; and 2) the computed flux gradually increased with increasing sample size until it converged to the measured flux when the sub-sample size was 20 mm by 20 mm or 400 mm^2.

Since full data sets for flow in discrete fractures are limited and expensive to obtain, the authors will make available to other researchers the full load and fracture deformation data set as well as the pore space data set and flow measurements for the discrete fracture sample that has been presented in this paper. An example of part of the pore space data set is presented in Appendix A. The full data set can be obtained by contacting Fracflow Consultants Inc. or the individual authors (eunjeong_ffc@nfld.net or john_ffc@nfld.net). Additional coupled stress and flow experiments that have been used to demonstrate the importance of using spatial variability data to accurately reproduce measured fracture flow data have included preliminary experiments on a 1 m by 1m by 1m fractured rock sample that was supplied by Dr. Alan Shapiro of the United States Geological Survey and simulation of inflow to a large underground mine [Seok, 2011]. In both cases the small scale or local variability was constrained by a second or larger scale level of spatial variability. The results [Seok, 2011] from both the large one metre scale fracture sample and the large underground mine inflow simulations demonstrate that modelling of flow measurements can be significantly improved by constructing the hydraulic conductivity input parameters using this spatial variability approach and that this approach is applicable to both small and large scale studies or simulations of both discrete fracture media and equivalent porous media

REFERENCES

Brace, W. F. (1980), Permeability of crystalline and argillaceous rocks. Int. J. Rock Mech. Min. Sci. & Geomech. Abstr., v. 17, pp. 241-251.

Brace, W. F. (1984), Permeability of crystalline rocks: New in situ meaurements. J. Geophys. Res., vol. 89, no. B8, pp. 4327-4330.

Bury, K. V. (1975), Statistical Models In Applied Science. John Wiley & Sons, New York, 625 p.
Clauser, C., 1992. Permeability of crystalline rocks. EOS, Trans. AGU, 73:21, pp. 233.

Diersch, H. -J. G. (2005), FEFLOW 5.3 Finite Element - Subsurface Flow and Transport Simulation System. WASY GnbH, Institute for Water Resources Planning and Systems Research, Berlin, Germany.

Duncan, J. M., P. A. Witherspoon, J. K. Mitchell, D. J. Watkins, J. H. Hardcastle and J. C. Chen (1972), Seepage and groundwater effects associated with explosive cratering. Report No. TE-72-2, University of California, Berkeley, 191 p.

Fracflow Consultants Inc. (1997), Relationship Between Fracture Pore Structure, Roughness, Solute Velocities and MBB1D Model Predictions. Report submitted to AECL Whiteshell Nuclear Research Laboratories, Pinawa, Manitoba.

Gale, J. E. (1984), Changes in fracture permeability as a function of sample size, fracture type, and stress history. IAH Int. Groundwater Symp. on Groundwater utilization and contaminant hydrogeology, Montreal, pp. 44-53.

Gale, J. E., 1987. Comparison of coupled fracture deformation and fluid flow models with direct measurements of fracture pore structure and stress-flow properties. Proceeding of 28th US Symposium on Rock Mechanics, Tucson, pp. 1213-1222.

Gale, J. E. (1993), Fracture properties from laboratory and large scale field tests: Evidence of scale effects. Proceedings of the Second International Workshop on Scale Effects in Rock Masses, Lisbon, Portugal, June 1993, (ISRM), pp. 341-352.

Gale, J. E. (1999), Impact of flow geometry, flow regime, two-phase flow and degassing on the transmissivity of rough fractures. SKB IPR-99-08, 126 p.

Gale, J. E. and K. G. Raven (1980). Effects of Sample Size on the Stress-Permeability Relationship for Natural Fractures. Technical Information Report No. 48, Swedish-American Cooperative Program on Radioactive Waste Storage in Mined Caverns in Crystalline Rock, Lawrence Berkeley Laboratory Report LBL-11865, Berkeley, 111 p.

Gale, J. E. and E. Seok (2004), Using Fracture Pore Space Geometry to Assess Degassing and Scaling Relationships in Fractured Rocks. Proceedings of the Second International Symposium on Dynamics of Fluids in Fractured Rock, February 10-12, 2004, pp. 25-26.

Gale, J. E., R. Macleod, J. Welhan, C. Cole and L. Vail (1987), Hydrogeological Characterization of the Stripa Site. SKB IPR-87-15.

Gale, J. E., R. A. Schaefer, A. B. Carpenter and A. Herbert (1991), Collection, analysis, and integration of discrete fractu qre data from the Monterey Formation for fractured reservoir simulations. 66th Annual Technical Conference and Exhibition of the Society of Petroleum Engineers, Dallas, Texas, October 6-9, 1991, SPE 22741, pp. 823-834.

Hubbert, M. K. (1956), Darcy's law and the field equations of the flow of underground fluids. Trans. Am. Inst. Min. Met. Engrs., v. 207, p. 222-239.

Louis, C. (1969), A study of groundwater flow in jointed rock and its influence on the stability of rock masses. Imperial College Rock Mechanics Research Report, No. 10, London, 88 p.

Margolin, Gennady, Brian Berkowitz & Harvey Scher (1998), Structure, flow, and generalized conductivity scaling in fracture networks. Water Resources Research, v. 34, no. 9, pp 2103-2121.

Neuman, Shlomo P. (1990), Universal scaling of hydraulic conductivities and dispersivities in geologic media. Water Resources Research, v. 26, no. 8, pp. 1749-1758.

Neuman, Shlomo P. (1994), Generalized Scaling of Permeabilities: Validation and Effect of Support Scale. Geophysical Research Letters, v. 21, no. 5, pp. 349-352.

Raven, K. G. and Gale, J. E. (1985), Water Flow in a Natural Rock Fracture as a Function of Stress and Sample Size. Int. J. Rock Mech. Min. Sci. & Geomech. Abstr. v. 22, no. 4, pp. 251-261.

Romm, E. S. (1966), Flow Characteristics of Fractured Rocks (in Russian). Nedra, Moscow, 283 p.

Seok, E. (2001), Pore space characterization and implications for flow simulation in discrete fracture planes. M.Sc. Thesis, Memorial University of Newfoundland, Canada, 166 p.

Seok, E. (2011), Impact of variability in laboratory and field fracture permeability data on simulated flux as a function of scale and spatial structure. Ph.D. Thesis, Memorial University of Newfoundland, Canada, 190 pages.

Witherspoon, Paul A. (2000), Investigations at Berkeley on Fracture Flow in Rocks: From the Parallel Plate Model to Chaotic Systems. Dynamics of Fluids in Fractured Rock, American Geophysical Union Geophysical Monotraph 122.

Witherspoon P. A., C. H. Amick, J. E. Gale, and K. Iwai (1979), Observations of a potential size effect in experimental determination of the hydraulic properties of fractures. Water Resour. Res. 15(5), pp. 1142- 1146.

Table 1(a) Distribution of the open pore space and the contact area for the ÄSPÖ2 samples (after Seok, 2001).

	ÄSPÖ2 - Measured
Total Number of Points	20152
Number of Open Pore Space Points	15124
Number of Contact Points	5028
Contact area (%)	24.95

Table 1(b) Basic statistics of the open pore space data (after Seok, 2001).

	ÄSPÖ2 - Measured
Mean, μ (mm)	0.2298
Std.Dev., σ (mm)	0.1638
Max. Aperture, σ (mm)	2.0790
μ_{LN} +	-1.6720
σ_{LN} +	0.6434
Skewness	-0.3920
μ_o * (mm)	0.2311
σ_o * (mm)	0.1655

+ μ_{LN} and σ_{LN} are the mean and standard deviation of the natural logarithm of the open pore space data.

* μ_o and σ_o are the mean and standard deviation of the original distribution, that were estimated with Equation (Bury, 1975, p. 279)

$$\mu_0 = \exp\left(\mu + \frac{\sigma^2}{2}\right) ; \quad \sigma_0 = \left\{\exp\left(2\mu + \sigma^2\right) \cdot \left[\exp\left(\sigma^2\right) - 1\right]\right\}^{1/2}$$

Table 2 Average of the apertures and corresponding equivalent porous media hydraulic conductivities used in the numerical modeling and the computed flux.

	Average 2b (mm)	Conductivity (m/s)	Flux (ml/s)
Uniform - 2b Arithmetic	0.173	2.03 E-4	1.4
Uniform - K Arithmetic	---	1.22 E-3	8.4
Uniform - 2b Geometric	0.051	5.20 E-6	0.03
Uniform - K Geometric	---	5.20 E-6	0.03
Random Distribution	0.173	Variable	0.33
Spatial Distribution	0.173	Variable	Range (0.43 - 0.56)

Table 3 Model geometry and input parameters.

Group Number	Number of sub-samples	Model Size (each sub-sample)	Grid Size	Injection Head (m)	Output Head (m)
SS10	30	10 mm x 10 mm	1 mm x 1 mm	2	1
SS15	30	15 mm x 15 mm	1 mm x 1 mm	2.5	1
SS20	30	20 mm x 20 mm	1 mm x 1 mm	3	1
SS30	30	30 mm x 30 mm	1 mm x 1 mm	4	1
SS40	27	40 mm x 40 mm	1 mm x 1 mm	5	1

Table 4 Simulation results.

Group Number	Mean of $Ln(Q_x^*)$	Min. of $Ln(Q_x^*)$	Max. of $Ln(Q_x^*)$	Mean of $Ln(Q_y^*)$	Min. of $Ln(Q_y^*)$	Max. of $Ln(Q_y^*)$	Mean of Ln(2b) (mm)
SS10	-8.47	-19.27	-1.49	-9.52	-19.33	-1.98	-3.25
SS15	-7.92	-19.04	-3.2	-7.72	-18.44	-2.97	-3.14
SS20	-6.19	-18.09	-3.67	-6.44	-17.97	-3.59	-2.88
SS30	-5.96	-17.39	-4.05	-6.43	-17.35	-3.82	-2.89
SS40	-5.75	-8.45	-3.74	-6.8	-17.76	-3.79	-2.94

Table A1 Raw Aperture Data Collected from Selected Sections of ASPO Sample.

- Fracture plane sample size: 190 mm x 290 mm
- Total number of section: 107
- Total number of data point: 20,152
- Aperture assigned on contact points: 0.001 mm

X Position mm	Y Position mm	Aperture mm
152	81	0.001
152.792	81	0.001
153.584	81	0.001
154.376	81	0.001
155.168	81	0.001
155.96	81	0.001
156.752	81	0.001
157.544	81	0.001
158.336	81	0.001
159.128	81	0.001
159.92	81	0.001
160.708	81	0.1052
161.507	81	0.0739
162.305	81	0.1643
163.103	81	0.1208
163.901	81	0.0013
164.693	81	0.001
165.485	81	0.001
166.277	81	0.001
167.079	81	0.1006
167.877	81	0.2349
168.676	81	0.1655
169.474	81	0.1876
170.272	81	0.1319
171.053	81	0.0799
171.832	81	0.0765
172.629	81	0.001

X Position mm	Y Position mm	Aperture mm
165.647	72.75	0.1442
166.447	72.75	0.001
167.239	72.75	0.001
168.031	72.75	0.001
168.848	72.75	0.0652
169.639	72.75	0.0348
170.448	72.75	0.1035
171.256	72.75	0.1324
172.065	72.75	0.1389
172.873	72.75	0.063
173.665	72.75	0.001
174.457	72.75	0.001
175.249	72.75	0.001
176.041	72.75	0.001
176.854	72.75	0.1278
177.662	72.75	0.0927
178.471	72.75	0.0459
179.281	72.75	0.0991
180.089	72.75	0.1373
180.898	72.75	0.1485
181.706	72.75	0.1641
182.515	72.75	0.1002
183.323	72.75	0.088
184.132	72.75	0.2818
184.94	72.75	0.1321
185.735	72.75	0.001
186.552	72.75	0.0834

X Position mm	Y Position mm	Aperture mm
9	11.185	0.001
9	11.989	0.001
9	12.793	0.001
9	13.597	0.001
9	14.401	0.001
9	15.205	0.001
9	16.009	0.001
9	16.813	0.001
9	17.617	0.001
9	18.421	0.001
9	19.225	0.001
9	20.029	0.001
9	20.833	0.001
9	21.637	0.001
9	22.441	0.001
9	23.245	0.001
9	24.049	0.001
9	24.853	0.001
9	25.629	0.001
9	26.402	0.1059
9	27.205	0.2088
9	28.008	0.2835
9	28.811	0.2902
9	29.614	0.2784
9	30.417	0.2186
9	31.22	0.1153
9	32.023	0.125

X Position mm	Y Position mm	Aperture mm
16.5	21.457	0.2107
16.5	22.262	0.1483
16.5	23.046	0.2219
16.5	23.852	0.453
16.5	24.657	0.4177
16.5	25.463	0.4797
16.5	26.268	0.7866
16.5	27.074	0.4733
16.5	27.879	0.313
16.5	28.684	0.001
16.5	29.46	0.0859
16.5	30.266	0.0941
16.5	31.07	0.001
16.5	31.872	0.1193
16.5	32.677	0.2181
16.5	33.483	0.1349
16.5	34.288	0.3626
16.5	35.094	0.4385
16.5	35.899	0.3327
16.5	36.705	0.094
16.5	37.498	0.1452
16.5	38.303	0.2904
16.5	39.109	0.1986
16.5	39.914	0.0606
16.5	40.725	0.1115
16.5	41.531	0.0797
16.5	42.336	0.3007

LIST OF FIGURES

Figure 17 Sub-samples with 40 mm by 40 mm size.

Figure 18 Schematic of bi-directional flow measurements, Qx for X direction and Qy for Ydirection.

Figure 19 Details of simulation results of each group - plot of logarithm of aperture and flux data.

Figure 20 Normalized flux and mean of apertures for each sub-sample.

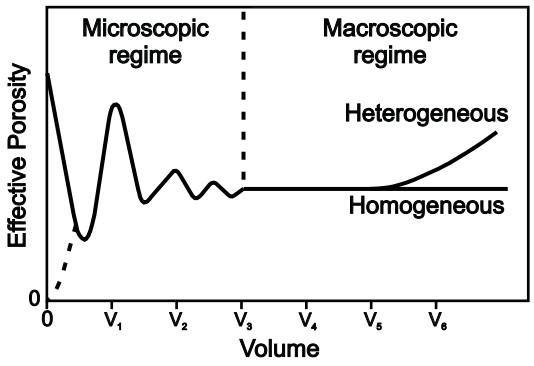

Figure 1 The representative elementary volume concept after Hubbert, 1956.

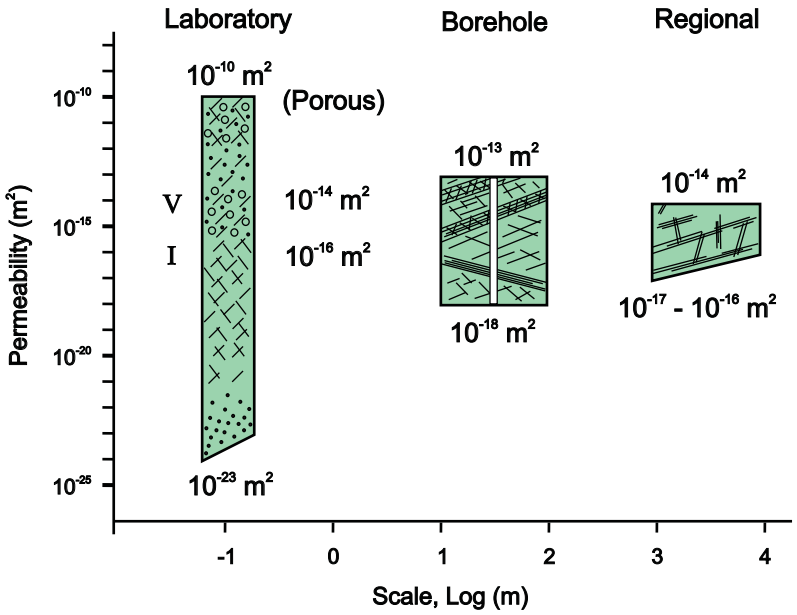

Figure 2 Range of permeability values for laboratory, borehole and regional scales, after Gale and Seok (2004) including data from Brace (1980 and 1984), Clauser (1992), Gale (1993), and Neuman (1994).

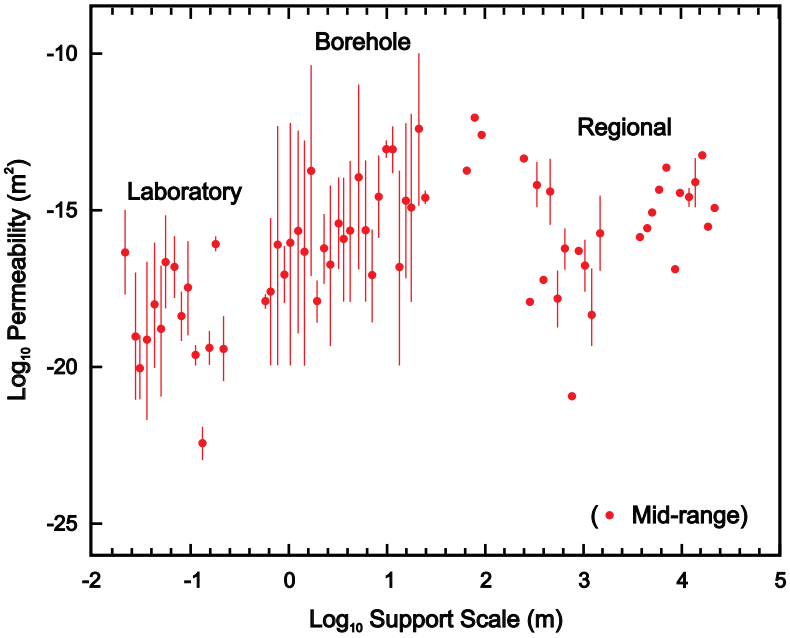

Figure 3 Permeability of crystalline rocks and characteristic scale of measurements (after Clauser, 1992).

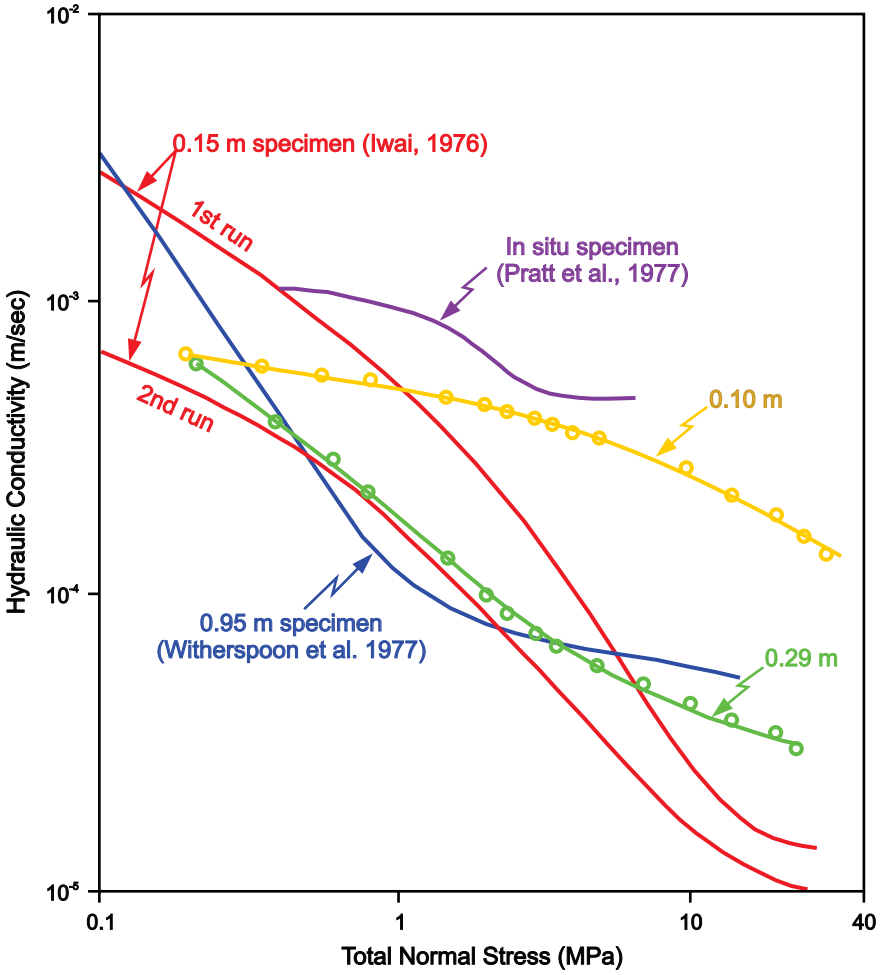

Figure 4 Comparison of the effect of sample size on the variation of fracture hydraulic conductivity with normal stress (Witherspoon et al. (1979) with data from Gale and Raven (1980)).

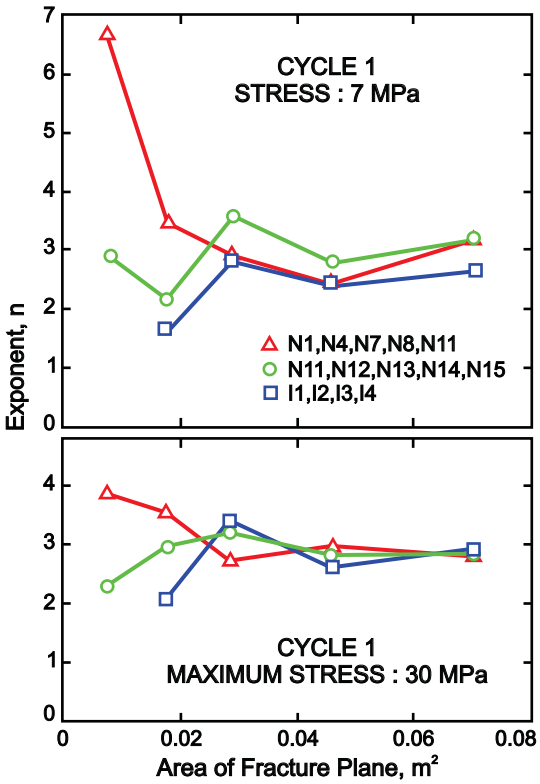

Figure 5 Plot of the exponent $(2b)^n$ from cycle 1 data for the thirteen samples at two of the reference stresses (7 MPa and 30 MPa) used to calculate the residual aperture (after Gale, 1984).

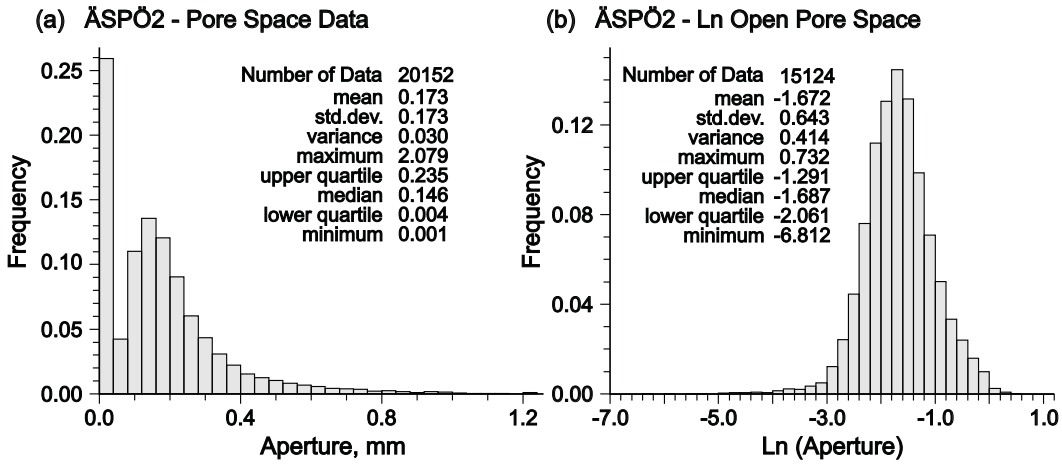

Figure 6 Histograms of the total pore space data (open pore space and contact area) for ÄSPÖ2 (a) and the logarithm of open pore space data for the ÄSPÖ2 sample (b) (after Seok, 2001).

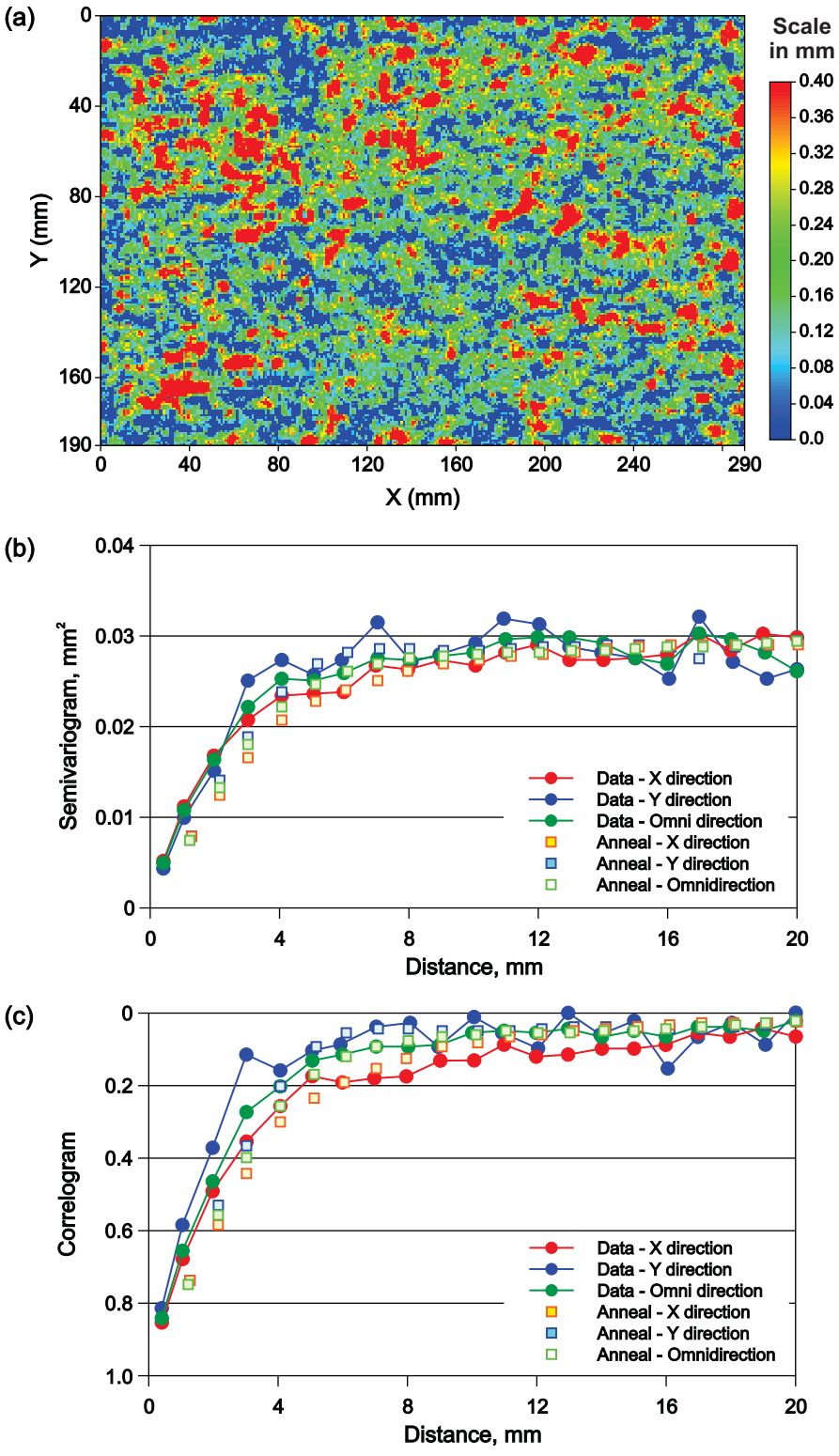

Figure 7 Pore space map (a), semivariogram (b) and correlogram (c) of the annealed data for ÄSPÖ2 (after Seok, 2001).

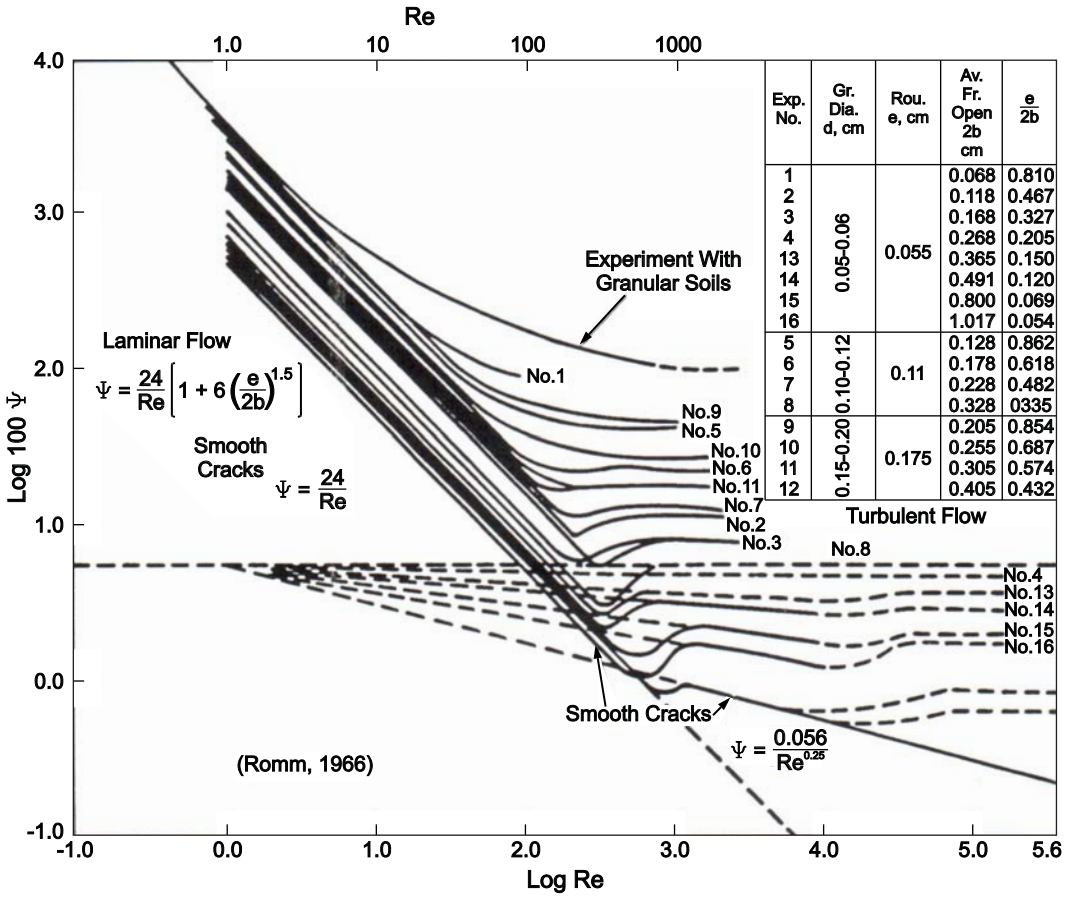

Figure 8 Effects of fluid velocity or Reynolds number on friction or head loss (after Gale, 1999. Original data from Romm, 1966).

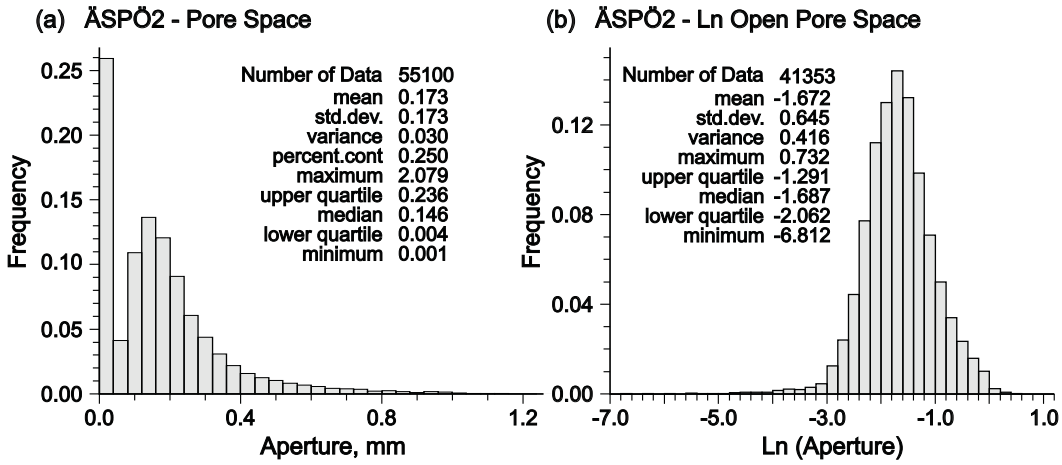

Figure 9 Histograms of the cartesian (a) and logarithm values (b) of the initial images for ÄSPÖ2 (after Seok, 2001).

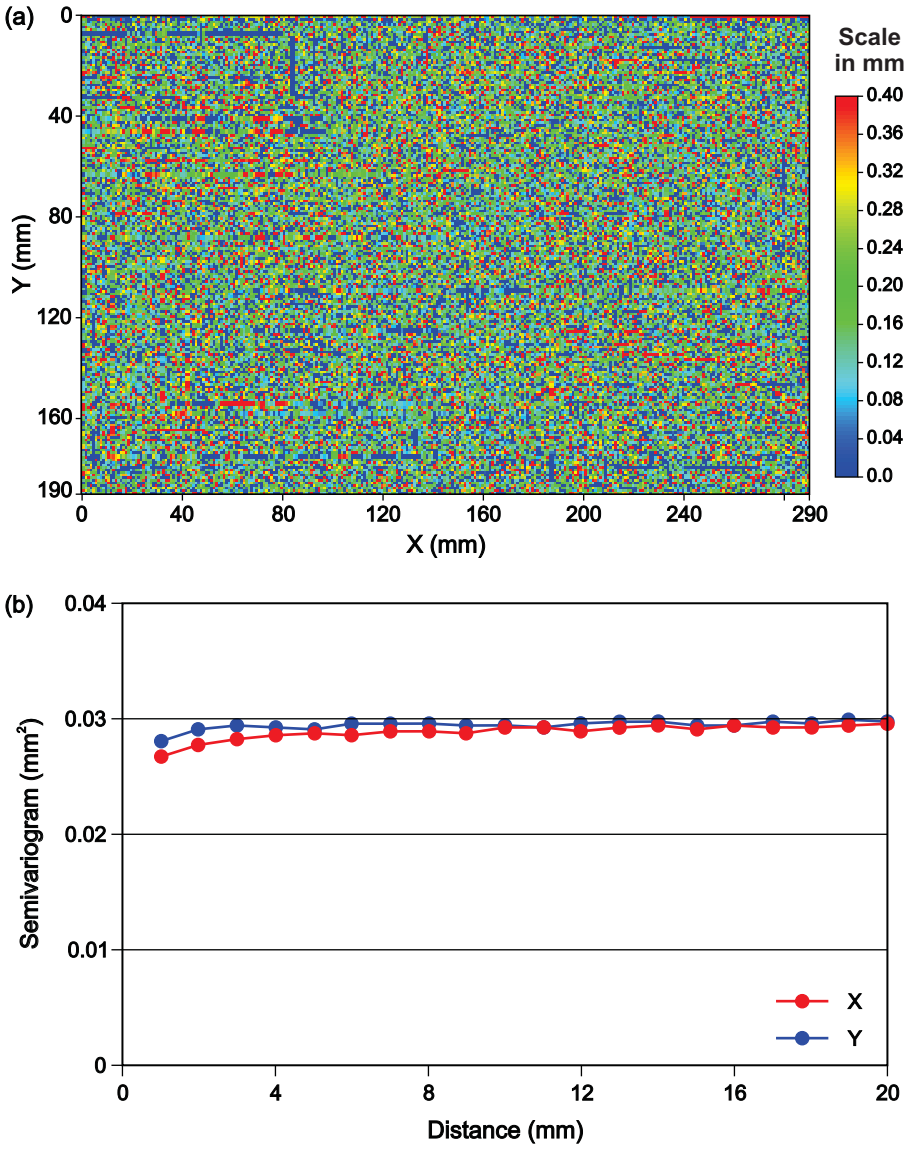

Figure 10 Pore space map (a) and semivariogram (b) of the initial image.

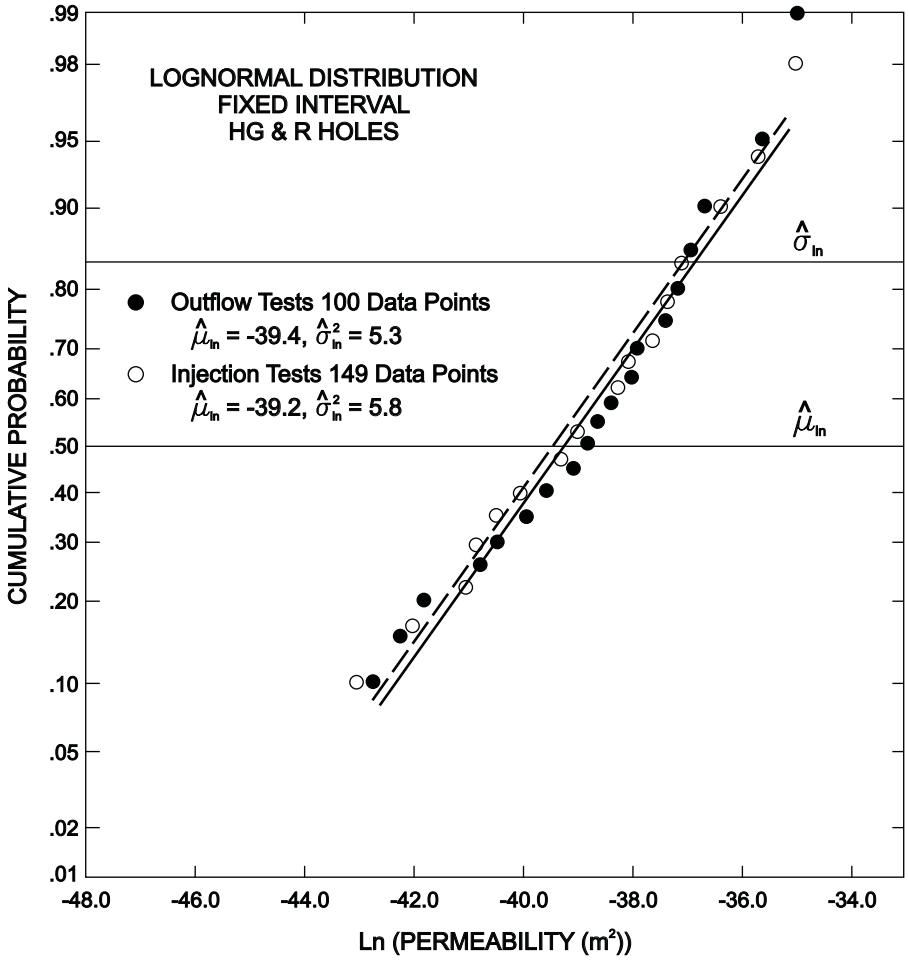

Figure 11 Lognormal distribution probability plot for fixed interval outflow and injection test permeabilities in the HG and R boreholes (after Gale et al., 1987).

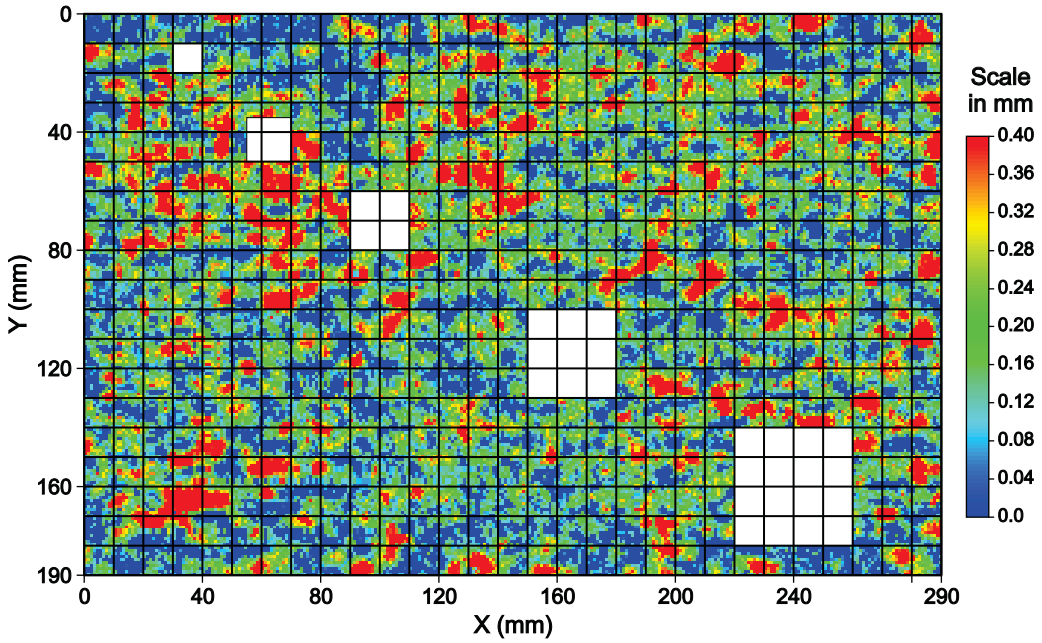

Figure 12 Selected sizes for sub-sampling, 10 mm, 15 mm, 20 mm, 30 mm and 40 mm rectangular.

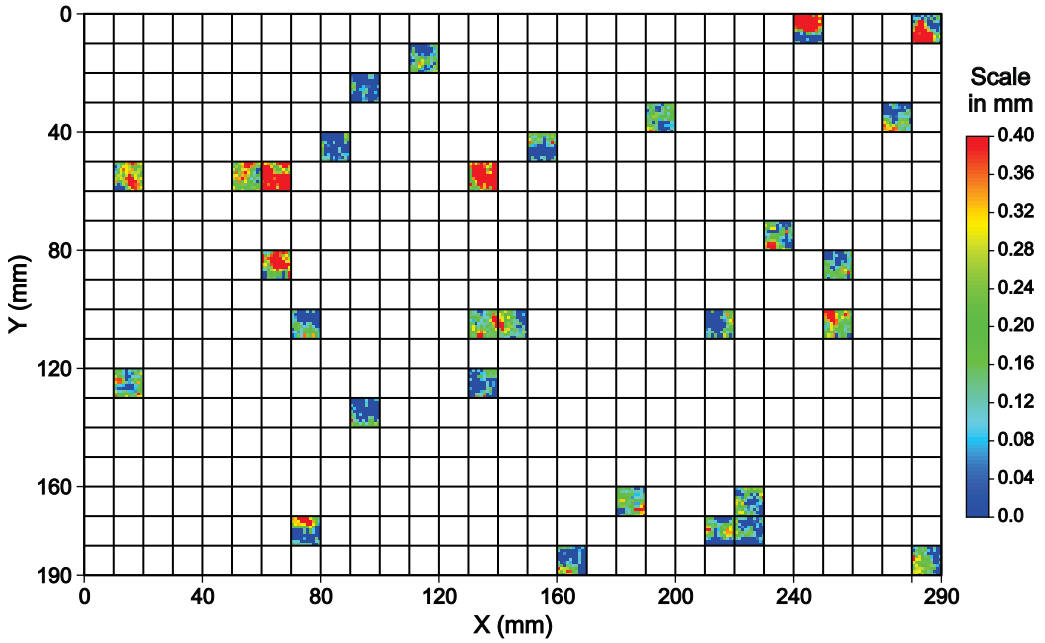

Figure 13 Sub-samples with 10 mm by 10 mm size.

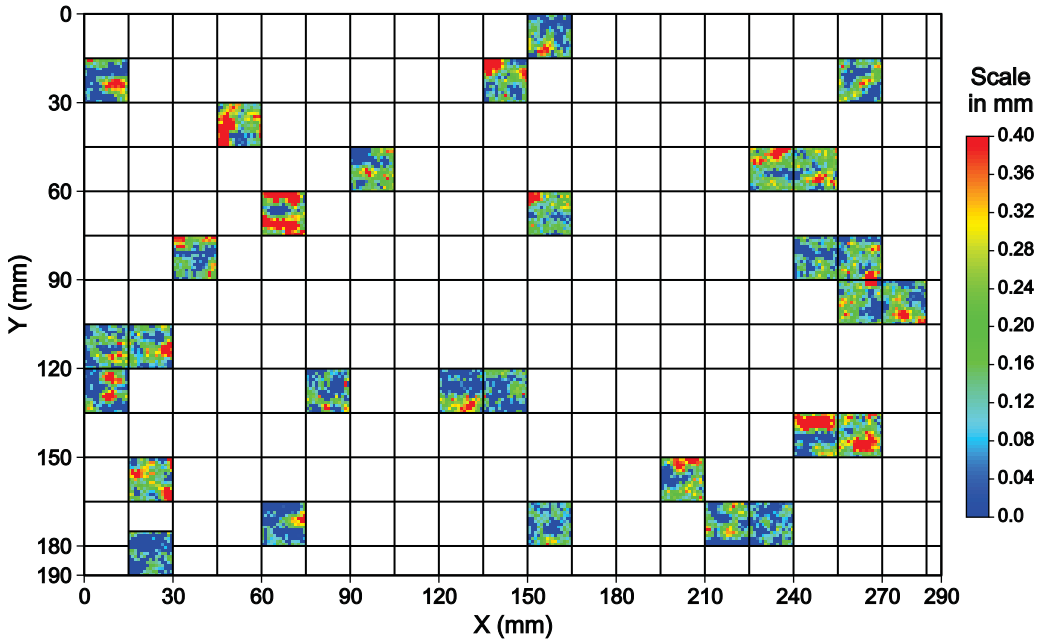

Figure 14 Sub-samples with 15 mm by 15 mm size.

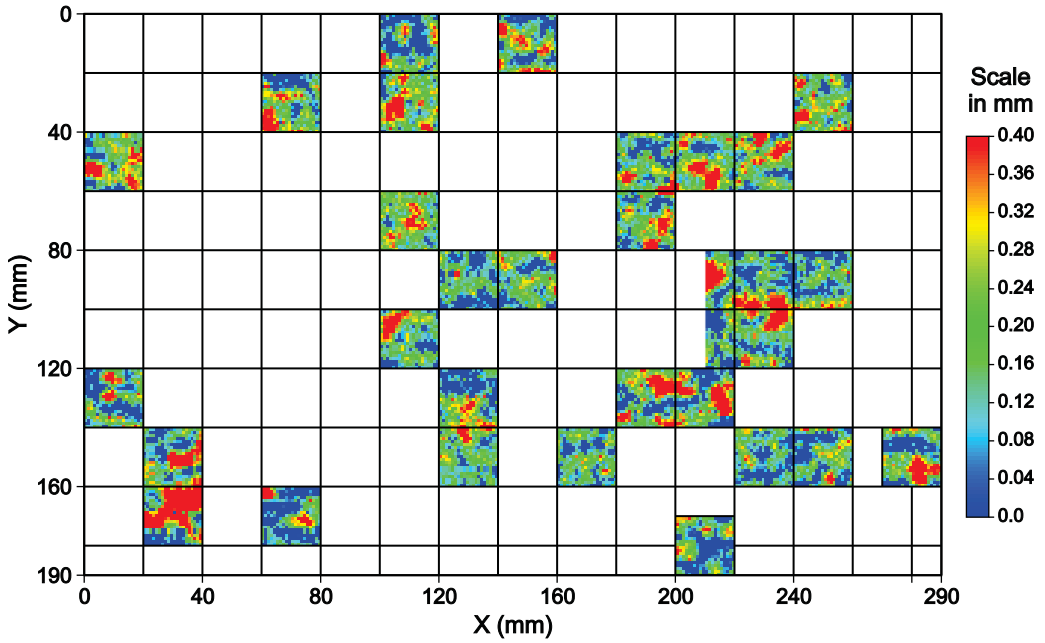

Figure 15 Sub-samples with 20 mm by 20 mm size.

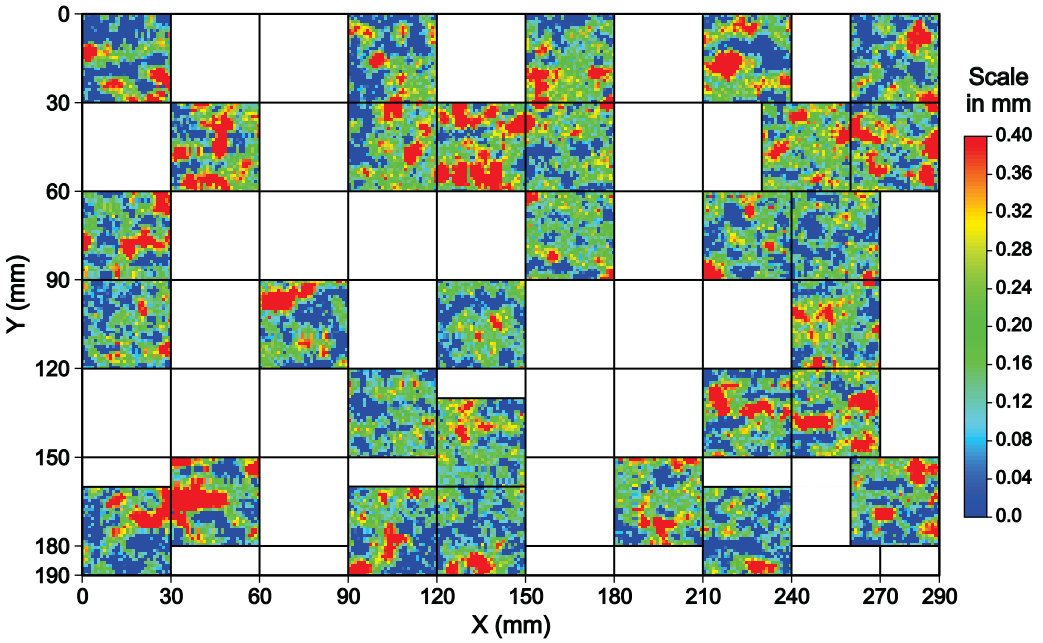

Figure 16 Sub-samples with 30 mm by 30 mm size.

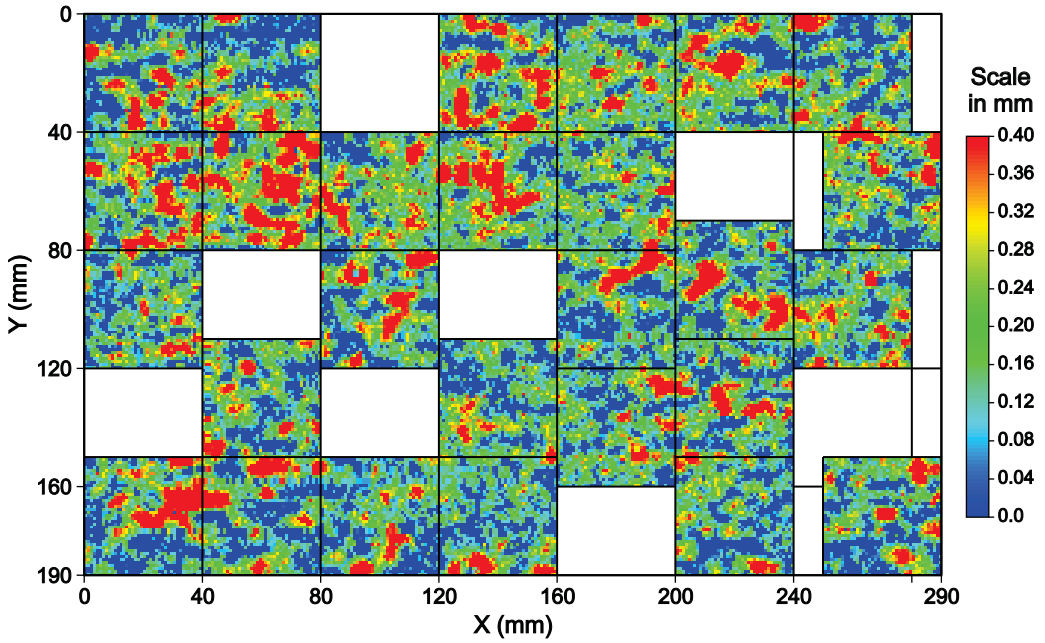

Figure 17 Sub-samples with 40 mm by 40 mm size.

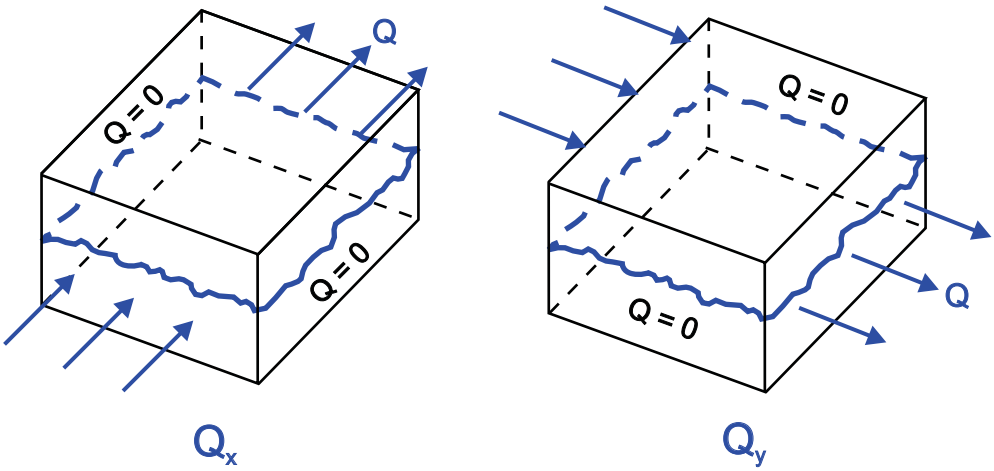

Figure 18 Schematic of bi-directional flow measurements, Q_x for X direction and Q_y for Y direction.

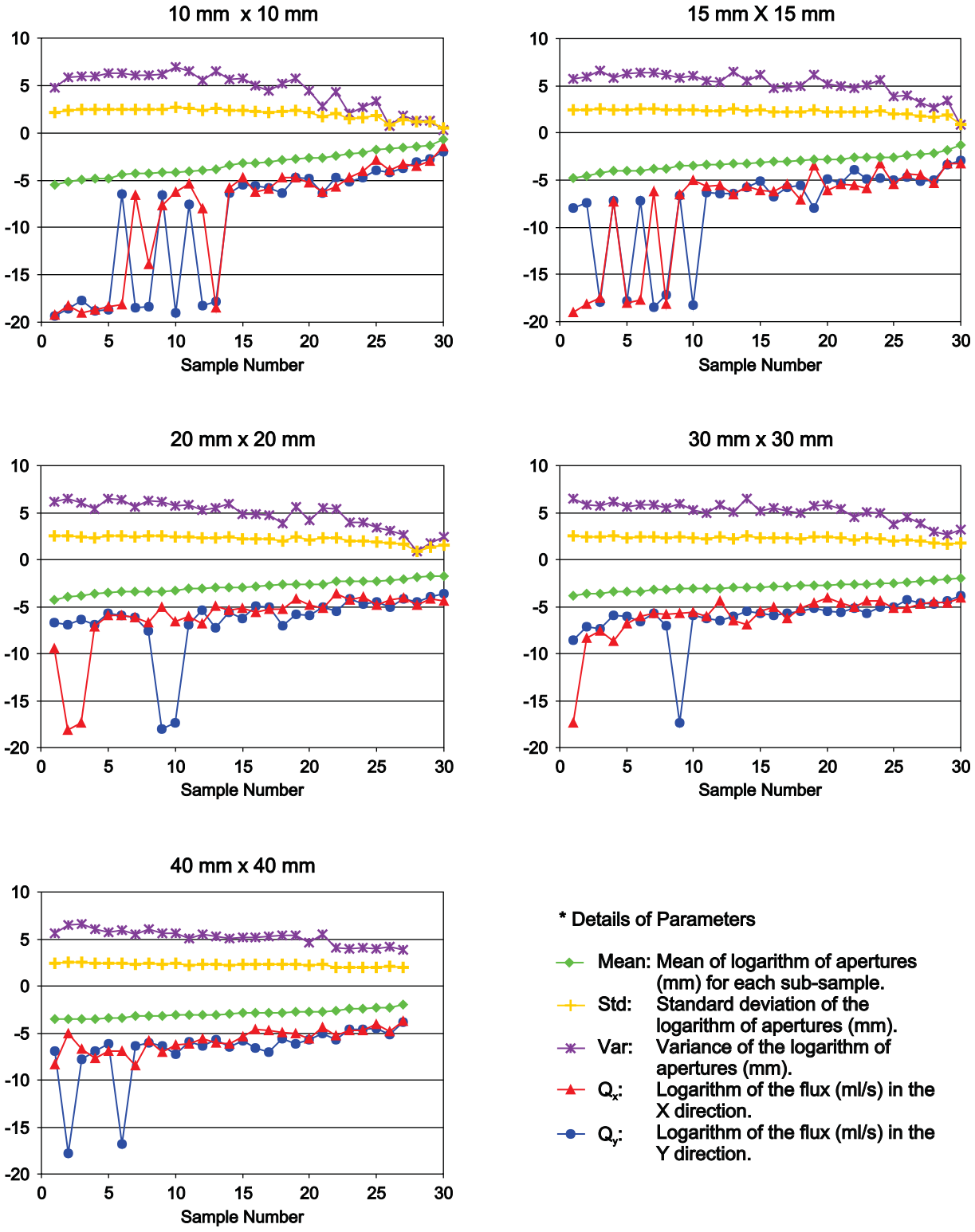

Figure 19 Details of simulation results of each group - plot of logarithm of aperture and flux data.

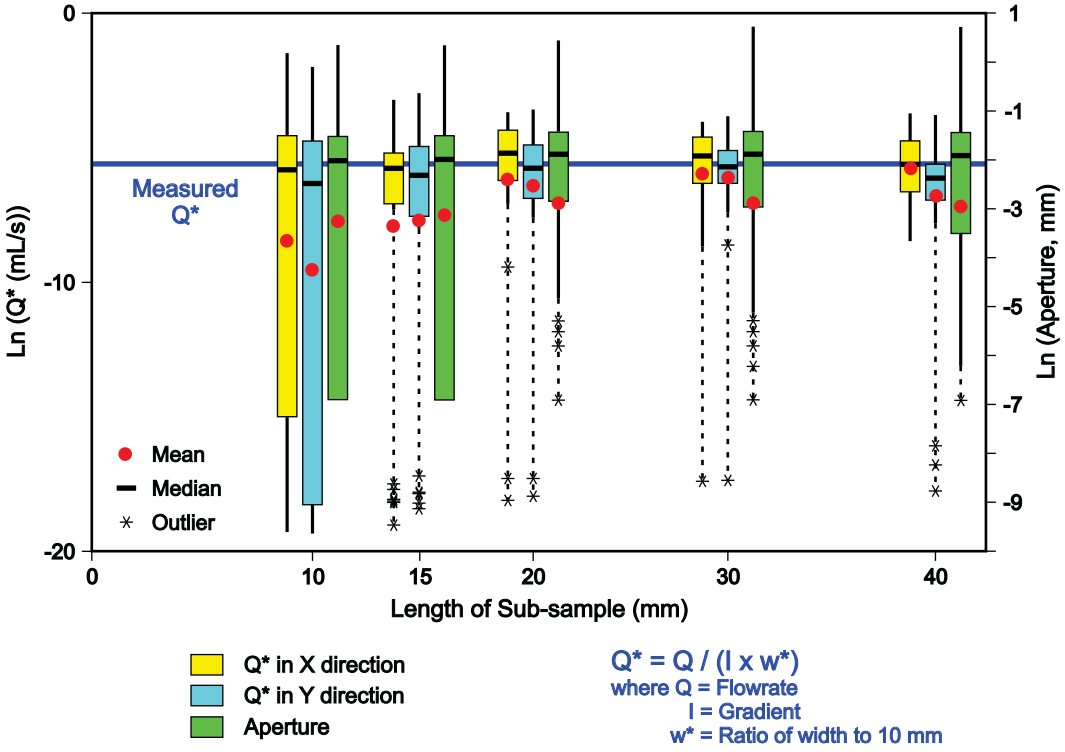

Figure 20 Normalized flux and mean of apertures for each sub-sample.